MATERIALS SCIENCE

Trace CO$_2$ capture by an ultramicroporous physisorbent with low water affinity

Soumya Mukherjee[1]*, Nivedita Sikdar[1]*, Daniel O'Nolan[1], Douglas M. Franz[2], Victoria Gascón[1], Amrit Kumar[1], Naveen Kumar[1], Hayley S. Scott[3], David G. Madden[1], Paul E. Kruger[3], Brian Space[2], Michael J. Zaworotko[1]†

CO$_2$ accumulation in confined spaces represents an increasing environmental and health problem. Trace CO$_2$ capture remains an unmet challenge because human health risks can occur at 1000 parts per million (ppm), a level that challenges current generations of chemisorbents (high energy footprint and slow kinetics) and physisorbents (poor selectivity for CO$_2$, especially versus water vapor, and/or poor hydrolytic stability). Here, dynamic breakthrough gas experiments conducted upon the ultramicroporous material SIFSIX-18-Ni-β reveal trace (1000 to 10,000 ppm) CO$_2$ removal from humid air. We attribute the performance of SIFSIX-18-Ni-β to two factors that are usually mutually exclusive: a new type of strong CO$_2$ binding site and hydrophobicity similar to ZIF-8. SIFSIX-18-Ni-β also offers fast sorption kinetics to enable selective capture of CO$_2$ over both N$_2$ (S_{CN}) and H$_2$O (S_{CW}), making it prototypal for a previously unknown class of physisorbents that exhibit effective trace CO$_2$ capture under both dry and humid conditions.

INTRODUCTION

Ever-increasing carbon dioxide (CO$_2$) levels in the atmosphere represent a global challenge for mankind (1, 2). CO$_2$ contributes to climate change (3), but atmospheric CO$_2$ is not only relevant to climate change but also a major health issue in confined spaces such as meeting rooms, aircraft, submarines, and spaceships, which can also suffer from elevated CO$_2$ concentrations. Whereas the specific concentrations of CO$_2$ that cause impairment of higher-order decision-making or long-term health risks remain uncertain (4), CO$_2$ capture (C-capture) devices are routinely deployed in spacecraft and submarines to control CO$_2$ concentration (5). Further, very recently, it was suggested that chronic exposure to levels as low as 1000 parts per million (ppm) can be harmful (6).

Generally, C-capture devices are the most expensive aspect of a C-capture, transport, and sequestration system because they exhibit high regeneration energy, require large equipment size, and result in equipment corrosion (7). While traditional C-capture technologies are suitable for large anthropogenic point sources where CO$_2$ levels are high, different approaches are required for mobile sources (8). C-capture using solid sorbents offers an energy-efficient alternative to traditional processes (9), but the challenge of C-capture is exacerbated for trace CO$_2$ removal from air [~400 ppm for direct air capture (DAC) and 1000 to 10,000 ppm for confined spaces] under variable conditions (gas composition, humidity level, and temperature). The sorbents currently used in indoor air quality (IAQ) control involve the use of activated carbon impregnated with MgO and/or CaO; C-capture occurs via chemical fixation of CO$_2$ as metal oxides transform to metal carbonates (10). A downside of this process lies with declined performance over repeated cycles (11). Further, the fact that CO$_2$ binding must be highly selective over atmospheric N$_2$ ($S_{CN} \geq 2500$) and H$_2$O ($S_{CW} \geq 100$) disqualifies all known physisorbent materials

from consideration (12, 13). Chemisorbents, on the other hand, are limited by poor sorption kinetics, energy-intensive regeneration, and chemical/thermal degradation on cycling (14).

The demand for energy-efficient solutions to trace gas separations has spurred research into porous metal-organic materials (MOMs) (15), also known as porous coordination polymers (16), or metal-organic frameworks (MOFs) (17). Unlike traditional classes of porous sorbents, these materials can be designed from first principles to afford control over pore size and chemistry. Unfortunately, MOFs, such as zeolites, typically lack the high selectivity and fast kinetics required for the removal of trace CO$_2$, in general, and from humid air, in particular (13). Many MOFs and zeolites are negatively affected by moisture (18, 19). Hybrid ultramicroporous materials (HUMs) (20), the current benchmarks for trace gas capture including C-capture (21) and acetylene capture (22), are also affected by humidity (18). The fact that the introduction of alkyl groups into pores can reduce the water affinity of MOMs (23) prompted us to study whether such an approach in HUMs might address the need for a porous material that combines (i) high affinity for CO$_2$ and (ii) low affinity for H$_2$O. Here, we report the first example of such a material.

RESULTS

[Ni(L)$_2$(SiF$_6$)]$_n$, L = 3,3′,5,5′-tetramethyl-1H,1′H-4,4′-bipyrazole, was prepared by hydrothermal reaction of L with NiSiF$_6$·6H$_2$O to afford a light blue powder, SIFSIX-18-Ni-α (Fig. 1A), an analog of SIFSIX-18-Cd (24). Heating SIFSIX-18-Ni-α to 85°C under vacuum induced a phase transition to SIFSIX-18-Ni-β (Fig. 1, B and C) and a 13.4% reduction in unit cell volume (see the Supplementary Materials for full details). Both forms of SIFSIX-18-Ni are primitive cubic (pcu) nets composed of two-dimensional layers of Ni(II) nodes cross-linked by organic linkers that are pillared by inorganic anions (SiF$_6^{2-}$). The resulting square channels are lined with inorganic anions, weakly basic nitrogen atoms, and methyl groups (Fig. 1B). After confirming bulk phase purity and crystallinity (Fig. 1C), particle size distribution analysis revealed a relatively uniform mean diameter of ca. 14 μm (Fig. 1D and fig. S6). Scanning electron microscopy revealed block-shaped morphology (Fig. 1D, inset).

[1]Bernal Institute, Department of Chemical Sciences, University of Limerick, Limerick V94 T9PX , Republic of Ireland. [2]Department of Chemistry, University of South Florida, 4202 East Fowler Avenue, CHE205, Tampa, FL 33620-5250, USA. [3]MacDiarmid Institute for Advanced Materials and Nanotechnology, School of Physical and Chemical Sciences, University of Canterbury, Private Bag 4800, Christchurch 8140, New Zealand.
*These authors contributed equally to this work.
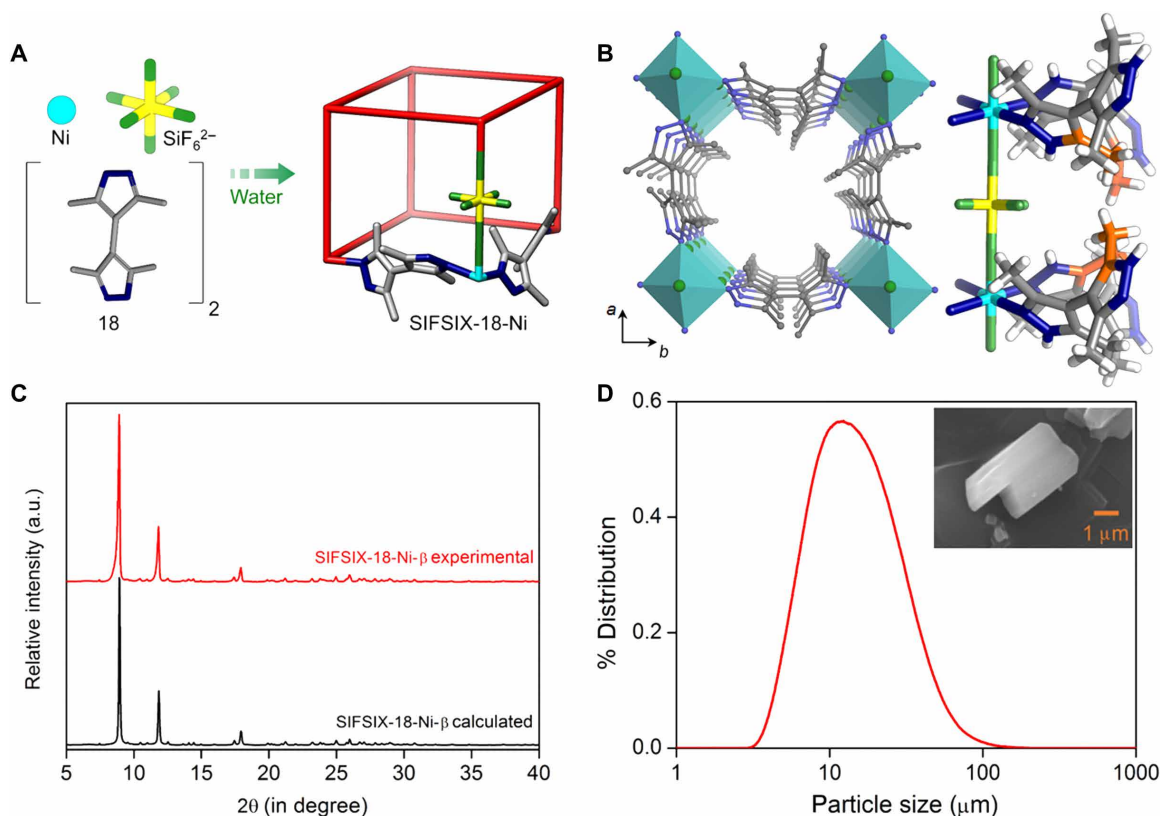†Corresponding author. Email: xtal@ul.ie

Fig. 1. Structure description, synthesis, and characterization. (**A**) Schematic illustration of the building blocks and pcu network topology of SIFSIX-18-Ni. (**B**) Left: View of the ultramicropore in SIFSIX-18-Ni-β along the crystallographic c axis (C, gray; N, blue; Si, yellow; F, green; Ni, cyan). Right: Illustration of the hydrophobic cavity (orange) decorated by methyl groups, amines, and inorganic pillars. (**C**) Experimental and calculated powder x-ray diffractograms of SIFSIX-18-Ni-β. (**D**) Particle size analysis and scanning electron microscopy image of SIFSIX-18-Ni-β crystals (inset). a.u., arbitrary units.

The sorption properties of SIFSIX-18-Ni-β were first examined using single-component isotherms (Fig. 2A and figs. S8 to S11). For comparative purposes, six additional physisorbent materials representing three classes of sorbents with strong potential for IAQ control were also evaluated: two MOFs [Mg-MOF-74, the benchmark MOF for C-capture (25), and ZIF-8, a hydrophobic MOF (26)], a zeolite that is known both as a desiccant and as a C-capture sorbent [Zeolite 13X (27)], and three HUMs that are known for their high CO_2 selectivity versus both N_2 and CH_4 [NbOFFIVE-1-Ni (28), TIFSIX-3-Ni (29), and SIFSIX-3-Ni (18, 19)] (Fig. 2, A and B, and figs. S13 to S18). The pure gas isotherms at CO_2 partial pressures relevant to DAC (ca. 500 ppm) and IAQ control (CO_2, 0.005 to 0.01 bar) reveal that only the HUMs exhibit strong C-capture performance. At 1000 ppm, CO_2 uptakes were as follows: NbOFFIVE-1-Ni and TIFSIX-3-Ni, 1.8 and 1.7 mmol g^{-1}, respectively; SIFSIX-18-Ni-β, SIFSIX-3-Ni, and Zeolite 13X, ca. 0.8 mmol g^{-1}; Mg-MOF-74 and ZIF-8, negligible. The HUMs were found to exhibit similar CO_2 sorption performance between 0.005 and 0.01 bar with near-full loading at 0.01 bar. Mg-MOF-74 and Zeolite 13X exhibited CO_2 uptakes of 0.9 (~13% loading) and 1.7 mmol g^{-1} (~28% loading) at 0.005 bar CO_2 and 298 K, respectively. No sorbent was observed to exhibit substantial N_2 uptake at 1.0 bar and 298 K (Table 1 and figs. S10 and S13 to S18).

With respect to H_2O sorption, Zeolite 13X (18.8 mmol g^{-1}), TIFSIX-3-Ni (7.5 mmol g^{-1}), NbOFFIVE-1-Ni (10.1 mmol g^{-1}) and SIFSIX-3-Ni (8.8 mmol g^{-1}) were found to exhibit high uptake at 95% relative humidity (RH). Conversely, ZIF-8 (2.6 mmol g^{-1}) and SIFSIX-18-Ni-β (1.6 mmol g^{-1}) exhibited low H_2O uptake consistent with surface sorption. Under ambient pressure, SIFSIX-18-Ni-β adsorbed 0.96 mmol g^{-1} at 95% RH (Fig. 2E) accompanied by a phase transition to SIFSIX-18-Ni-α [in situ powder x-ray diffraction (PXRD); fig. S5], however regenerable by temperature swing. Mg-MOF-74 was not studied due to its hydrolytic instability (18, 30).

The isosteric heat of adsorption (Q_{st}) values for CO_2 are generally flat across the range of loading and decrease in line with the low pressure uptakes reported above: NbOFFIVE-1-Ni (54 kJ mol^{-1}) > SIFSIX-18-Ni-β (52 kJ mol^{-1}) > TIFSIX-3-Ni (50 kJ mol^{-1}) > SIFSIX-3-Ni (45 kJ mol^{-1}) > Mg-MOF-74 (42 kJ mol^{-1}) > Zeolite 13X (39 kJ mol^{-1}) > ZIF-8 (26.7 kJ mol^{-1}) (Fig. 2C, Table 1, figs. S19 and S20, and tables S2 and S3) (29). Gravimetric CO_2 adsorption at 1 bar/303 K revealed that whereas SIFSIX-18-Ni-β, NbOFFIVE-1-Ni, TIFSIX-3-Ni, and SIFSIX-3-Ni exhibit lower CO_2 uptake than Mg-MOF-74 and Zeolite 13X, they offer superior kinetics, reaching 90% of their equilibrium loading within ca. 1 min of exposure versus 20 to 40 min (Fig. 2D). Under dry/wet trace CO_2/N_2 mixtures, the C-capture kinetics of SIFSIX-18-Ni-β even outperforms the benchmark silica chemisorbent TEPA-SBA-15 (figs. S53 and S54) (31). Selectivity determined via ideal adsorbed solution theory (IAST) (32) revealed that, at 298 K, SIFSIX-18-Ni-β in effect serves as a partial sieve for S_{CN} (figs. S9 and S45). The IAST selectivity for S_{CW}, which was calculated at 74% RH and 500 ppm CO_2, is 16.2, with higher S_{CW} values of 54.0 and 173.1 at 0.005 and 0.01 bar CO_2, respectively (table S1
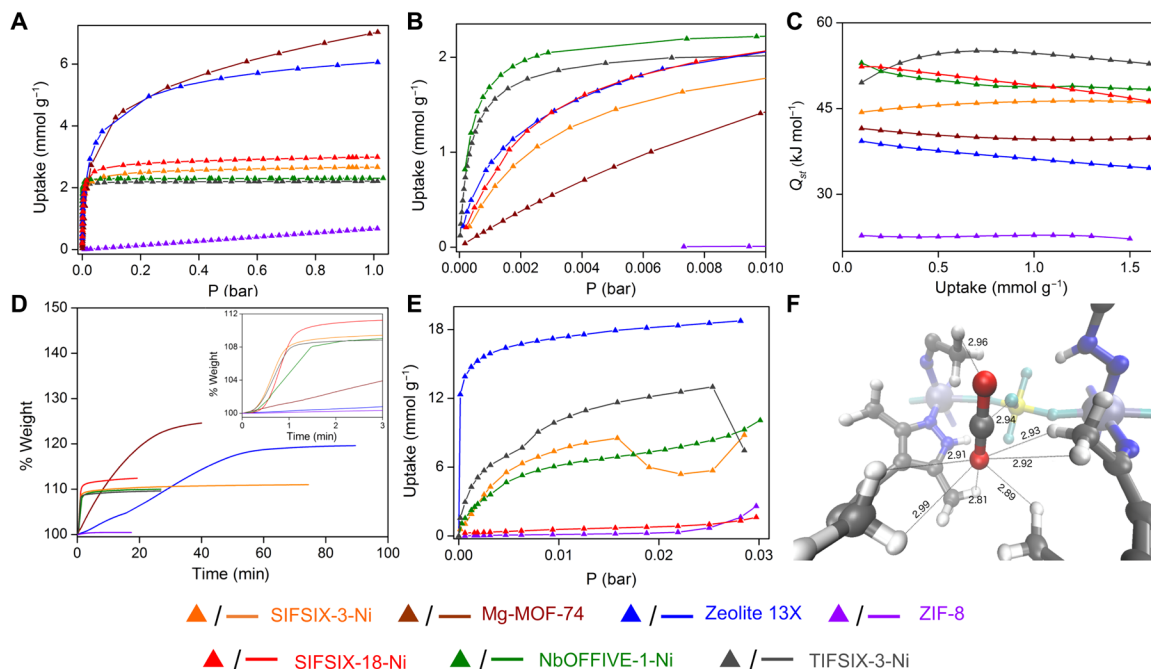
Fig. 2. Single-component sorption, kinetic studies, and "sweet spot" for CO2 binding. (**A** and **B**) Low-pressure CO2 isotherms at 298 K. (**C**) Isosteric heat of adsorption profiles for CO2. (**D**) Gravimetric CO2 uptake (1.0 bar) versus time at 303 K. (**E**) Dynamic vapor sorption (DVS) isotherms for H2O at 298 K. (**F**) CO2 binding sites in SIFSIX-18-Ni-β determined by ab initio periodic computation. Dashed lines indicate CO2--HUM internuclear distances from 2.81 to 2.99 Å. Color code: C, gray; H, white; O, red; N, sapphire; Si, yellow; F, cyan; Ni, light blue.

Table 1. Isosteric heat of adsorption, gas sorption, and selectivity data.

Material	CO2 Q_{st} (kJ mol^{-1})*	CO2 uptake (298 K) (mmol g^{-1})					N2 (298 K, 1 bar) mmol (g^{-1})	H2O (298 K, 95% RH) (mmol g^{-1})†	IAST selectivity‡	
		500 ppm	1000 ppm	3000 ppm	5000 ppm	10,000 ppm			S_{CN}§	S_{CW}‖
Mg-MOF-74	42	0.05	0.2	0.5	0.9	1.6	0.85	~33.33¶	238	N/A
Zeolite 13X	39	0.4	0.9	1.4	1.7	2.0	0.42	18.76	562	N/A
SIFSIX-18-Ni-β	52	0.4	0.8	1.4	1.8	2.2	0.04	1.64/0.96#	N/A**	16.2‡‡
SIFSIX-3-Ni	45	0.4	0.7	1.2	1.5	1.8	0.16	8.80	1438	N/A††
NbOFFIVE-1-Ni	54	1.3	1.8	2.0	2.1	2.3	0.15	10.09	6528	0.03‡‡
TIFSIX-3-Ni	49	1.2	1.7	1.9	1.9	2.0	0.18	7.46	8090	N/A††
ZIF-8	27	~0.0006	<0.005	<0.005	0.006	0.01	0.1	1.44#	3.1	0.08

*Virial fitting of CO2 sorption data collected between 0 and 10 mbar. †Data collected on surface measurement systems vacuum DVS unless otherwise stated. ‡Selectivity for sorbents was determined by interpolation of raw isotherm data points (see the Supplementary Materials for further details). §Selectivity based upon 500 ppm CO2 concentration. ‖Selectivity based upon 500 ppm CO2 concentration/74% RH. ¶Water uptake for Mg-MOF-74 was acquired from (30). #Water uptake based upon surface measurement systems intrinsic DVS data. **IAST selectivity suggests partial sieving (see the Supplementary Materials). ††IAST cannot be calculated due to negative adsorption observed as a result of phase change in the presence of water. ‡‡Calculated at 74% RH and 500 ppm.

and figs. S25 and S26). These S_{CW} values are not corrected for surface sorption and are likely to be even higher. In summary, SIFSIX-18-Ni-β is, to our knowledge, the first physisorbent that combines strong C-capture performance and low water uptake.

To understand its unexpectedly strong C-capture properties, we modeled the CO2 binding site in SIFSIX-18-Ni-β by ab initio and empirical simulations. The empirically modeled structure of a 2 × 2 × 2

box of unit cells of SIFSIX-18-Ni-β (fig. S57) revealed a series of CH···O interactions supplementing the expected C···F binding between the electropositive carbon atoms of CO2 and fluorine moieties of SIFSIX (Fig. 2F). The initial binding site for CO2 from ab initio periodic computation resembles that in other SIFSIX systems in that there is an interaction with a SIFSIX moiety (C_{CO2} − F_{SIFSIX} = 2.94 Å; Fig. 2F). However, the binding site is otherwise distinct in that there

are also electrostatic attractions between the partially negative O atoms of CO_2 and partially positive methyl hydrogen atoms of SIFSIX-18-Ni-β. In addition, empirical simulations revealed a $C_{CO2} – F_{SIFSIX}$ distance of as low as 2.54 Å at 298 K. Concurrent $O_{CO2} – H_{HUM}$ interactions of 2.81, 2.89, 2.91, 2.92, 2.93, 2.96, 2.99, and 3.09 Å were also found in the optimized structure (see the Supplementary Materials for full details). This binding site more resembles the type of binding site typically found in enzymes than that of other HUMs.

Real-time trace C-capture performance for each physisorbent was examined via fixed-bed column breakthrough experiments (Fig. 3, A to F; figs. S27 to S40; and table S4) using binary CO_2/N_2 mixtures that mimic indoor CO_2 concentrations: 1000/3000 ppm, 298 K, dry/74% RH (4). The dry 1000 ppm CO_2 saturation uptake of SIFSIX-18-Ni-β was observed to be 0.7 mmol g^{-1} with a breakthrough retention time of 715 min g^{-1} (Fig. 3A and fig. S27). TIFSIX-3-Ni offered the best dry 1000 ppm CO_2 saturation uptake and breakthrough retention time of the sorbents studied (1.6 mmol g^{-1} and 1670 min g^{-1}, respectively) (Fig. 3A). However, at 74% RH, SIFSIX-18-Ni-β was found to be the top performing material with CO_2 saturation uptake of 0.3 mmol g^{-1} and a breakthrough time of ca. 260 min g^{-1}; the performance of the other sorbents studied was degraded by >80% humidity (Fig. 3B). For the dry 3000 ppm CO_2/N_2 experiments, the CO_2 sorption performances of TIFSIX-3-Ni and Zeolite 13X are comparable with saturation uptakes and breakthrough retention times of ca. 2.1 mmol g^{-1} and 700 min g^{-1}, respectively (Fig. 3C and table S4). Under the same conditions, CO_2 saturation uptakes for SIFSIX-18-Ni-β (ca. 1.5 mmol g^{-1}), NbOFFIVE-1-Ni (ca. 1.9 mmol g^{-1}), SIFSIX-3-Ni (ca. 1.6 mmol g^{-1}), and ZIF-8 (ca. 0.002 mmol g^{-1}) (retention times for the first three: ca. 520, 425, and 322 min g^{-1}, respectively) were

observed. However, at 74% RH, the performance of both NbOFFIVE-1-Ni and Zeolite 13X deteriorated with CO_2 saturation uptakes of only 0.5 and 0.1 mmol g^{-1}, respectively (retention times: ca. 128 and 20 min g^{-1}, respectively) (Fig. 3D). Under the same conditions, SIFSIX-18-Ni-β, TIFSIX-3-Ni, and SIFSIX-3-Ni stand out from Zeolite 13X and NbOFFIVE-1-Ni with CO_2 saturation uptakes of 0.8, 0.8, and 0.9 mmol g^{-1}, respectively. Notably, the CO_2 retention time for SIFSIX-18-Ni-β (ca. 316 min g^{-1}) was greater than those of SIFSIX-3-Ni and TIFSIX-3-Ni (ca. 187 and 283 min g^{-1}, respectively).

NbOFFIVE-1-Ni and SIFSIX-18-Ni-β, the top performing sorbents, were further subjected to 5000 ppm/99.5% and 10,000 ppm/99% CO_2/N_2 breakthrough experiments (figs. S39 and S40). For SIFSIX-18-Ni-β, CO_2 saturation uptakes (dry/wet) were found to be 1.7/1.2 mmol g^{-1} at 5000 ppm (retention times, 735/532 min g^{-1}, respectively) and 2.0/1.7 mmol g^{-1} at 10,000 ppm (retention times, 440/410 min g^{-1}, respectively). For NbOFFIVE-1-Ni, the CO_2 saturation uptakes were lower under dry conditions and much lower under wet conditions: 1.5/0.7 mmol g^{-1} at 5000 ppm (retention times, ca. 650/333 min g^{-1}, respectively) and 1.8/1.1 mmol g^{-1} at 10,000 ppm (retention times, ca. 340/255 min g^{-1}, respectively). The performance of NbOFFIVE-1-Ni at 0.01 bar (10,000 ppm) is consistent with a previous report (28). Table S4 tabulates the breakthrough results at all CO_2 levels and reveals that SIFSIX-18-Ni-β is much less affected by the presence of moisture than the other C-capture sorbents at all levels from 1000 to 10,000 ppm.

The stability of SIFSIX-18-Ni-β was evaluated using an accelerated stability protocol adopted by the pharmaceutical industry (storage at 40°C and 75% RH) (33). PXRD data revealed that SIFSIX-18-Ni-β reverted to the α polymorph after 14 days, but it is regenerable
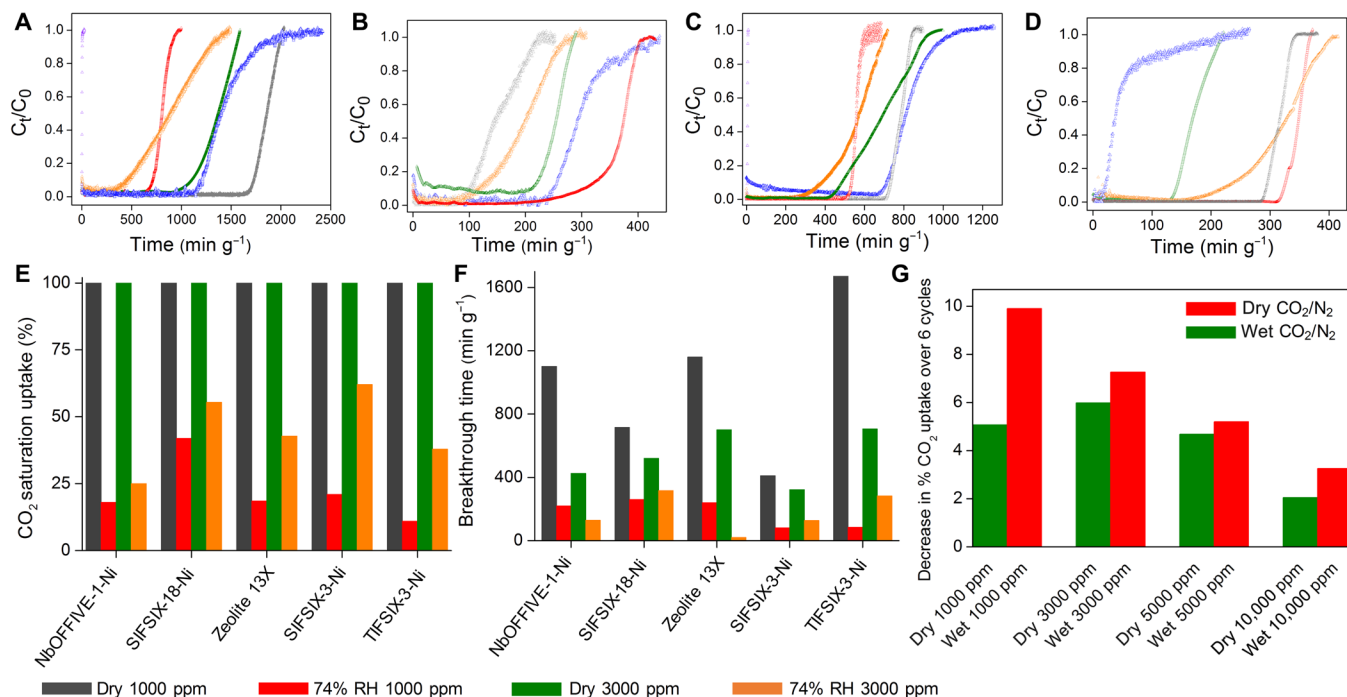

Fig. 3. Dynamic gas breakthrough and recyclability tests. Dynamic gas breakthrough tests for SIFSIX-18-Ni-β (red), NbOFFIVE-1-Ni (green), Zeolite 13X (blue), SIFSIX-3-Ni (orange), TIFSIX-3-Ni (gray), and ZIF-8 (purple) using (**A**) dry 1000 ppm, (**B**) 74% RH 1000 ppm, (**C**) dry 3000 ppm, and (**D**) 74% RH 3000 ppm CO_2/N_2 [v/v = 0.1/99.9% for (A) and (B) and v/v = 0.3/99.7% for (C) and (D)] gas mixtures (298 K; 1 bar; flow rate, 20 cm^3 min^{-1}). (**E**) Bar diagram exhibiting the relative decline in CO_2 saturation uptakes (%) of SIFSIX-18-Ni-β versus other physisorbents (dry/74% RH, 1000/3000 ppm CO_2/N_2). (**F**) Bar diagram of CO_2 retention times (min g^{-1}) under dry/74% RH, 1000/3000 ppm CO_2/N_2. (**G**) Decrease in % CO_2 uptakes over six consecutive adsorption-desorption cycles for SIFSIX-18-Ni-β (CO_2/N_2 dry/wet gas mixtures of the following composition: 1000, 3000, 5000, and 10,000 ppm CO_2, without/with 74% RH, saturated with N_2).

(fig. S42) with negligible change in BET surface area and CO_2 sorption performance (figs. S43 and S44). To further examine recyclability of SIFSIX-18-Ni-β, we conducted 100 adsorption/desorption cycles in the presence of 1.0 bar CO_2 at 308 K (fig. S52). Full loading was achieved in each cycle after ca. 1 min; desorption experiments were performed at 348 K to ensure regeneration. SIFSIX-18-Ni-β exhibited no loss in performance over 100 cycles under these conditions. Similar results under dry and wet (74% RH) CO_2/N_2 mixtures with CO_2 concentrations of 1000, 3000, 5000, and 10,000 ppm (Fig. 3G and figs. S48 to S51) further validated the trace C-capture performance. The fact that effluent CO_2 levels are <50 ppm across all trace C-capture conditions (table S4) qualifies SIFSIX-18-Ni-β as a sorbent suitable for IAQ needs.

DISCUSSION

Whereas the use of physisorbents for trace C-capture offers a potentially superior alternative to traditional processes (34), even the top performing physisorbents such as zeolites and MOFs lack the selectivity and/or kinetics needed for trace C-capture under dry conditions. Further, the performances of NbOFFIVE-1-Ni and Mg-MOF-74 are degraded by their strong affinity for H_2O. Conversely, hydrophobic MOFs such as ZIF-8 exhibit low H_2O uptake but suffer from very low CO_2 uptake and/or selectivity. In essence, a *Catch-22* situation exists: Pore surfaces with the requisite thermodynamics and kinetics to address trace level C-capture tend to also have binding sites that enable high water uptake (e.g., NbOFFIVE-1-Ni; figs. S21, S22, S29, and S30) (29, 35); hydrophobic pore surfaces that offer low water uptake tend to also exhibit low CO_2 affinity (e.g., ZIF-8). In this context, SIFSIX-18-Ni-β represents a paradigm shift in terms of both properties and pore design. With respect to properties, SIFSIX-18-Ni-β combines unexpectedly strong affinity for CO_2 along with the hydrophobicity that we anticipated from its methyl-decorated pores (36). With respect to design, the CO_2 binding site presents two synergistic features: a relatively strong C⋯F interaction to a SIFSIX moiety and six weak C-H⋯O interactions from methyl groups. This "pocket" (Figs. 1B and 2F and fig. S57) for CO_2 enables a binding interaction (52 kJ mol^{-1}) that approaches that of the leading physisorbents, NbOFFIVE-1-Ni and TIFSIX-3-Ni, but offers only weak interactions with O_2, N_2 and notably, H_2O.

The mechanism of C-capture in SIFSIX-18-Ni-β is therefore unlike other physisorbents that offer strong C-capture performance, which tend to bind CO_2 through open metal sites or strong electrostatic environments or via chemical reaction with amine groups (37). Rather, the binding site in SIFSIX-18-Ni-β has enzyme-like features that result in a tight CO_2 binding. A similar situation exists in $[Zn_2(Atz)_2(ox)]_n$, which exploits supramolecular interactions that offer a strong interaction with CO_2 (40.8 kJ mol^{-1}) but weak interactions toward N_2, H_2, and Ar (38). SIFSIX-18-Ni-β teaches a further message that is also offered by nature's predominant carbon-fixing enzyme, ribulose-1,5-bisphosphate carboxylase/oxygenase (RuBisCo), which must also sequester CO_2 in humid environments. The key to RuBisCo's C-capture performance is thought to lie with its small hydrophobic side chains that enable a cavity that concentrates CO_2 (39). Nevertheless, despite the critical role that RuBisCo plays in the global carbon cycle, it suffers from relatively inefficient performance that would render it ineffective for industrial C-capture: low density of CO_2 binding sites, competitive binding by O_2, and slow kinetics (40). SIFSIX-18-Ni-β also presents a hydrophobic pocket that addresses the need for weak H_2O binding, but it otherwise offers key performance advantages over RuBisCo: very high CO_2/O_2 selectivity (molar $S_{CO} \sim 2079$ for 10,000 ppm $CO_2/99\% O_2$, fig. S11; IAST $S_{CO} > 3 \times 10^4$ suggested sieving, fig. S46), fast CO_2 sorption kinetics (Fig. 2D), and a relatively high density of binding sites. Further, in situ PXRD (fig. S4), Fourier transform infrared (FTIR) measurement (fig. S47), and cycled kinetic adsorption experiments (Fig. 3G and fig. S52) reveal that CO_2 sorption in SIFSIX-18-Ni-β is facile, as temperature swing recycling can be conducted at 348 K (figs. S23 and S41). These features mean that, unlike existing benchmark physisorbent materials, the C-capture performance of SIFSIX-18-Ni-β is retained even at high RH in 0.005 bar (0.5% CO_2) and 0.01 bar (1% CO_2) CO_2 gas mixtures (figs. S39 and S40).

CONCLUSIONS

A crystal engineering approach to pore size (ultramicroporosity) and pore chemistry (coupling of strong electrostatic interactions from inorganic anions and hydrophobicity from methyl groups) control has resulted in a HUM, SIFSIX-18-Ni-β, with binding sites that exhibit exceptional CO_2 selectivity from wet CO_2/N_2 gas mixtures. SIFSIX-18-Ni-β thereby offers highly effective C-capture performance under conditions that mimic C-capture from air in confined spaces and presents an energy-efficient potential solution to IAQ control. The nature of the binding site in SIFSIX-18-Ni-β is key to its performance and provides insight into how to generally improve the performance of physisorbents with respect to C-capture when CO_2 is present at trace levels in humid gas mixtures.

MATERIALS AND METHODS
Gas sorption measurements

Ultrahigh-purity gases, as received from BOC Gases [research-grade He (99.999%), CO_2 (99.995%), O_2 (99.999%), and N_2 (99.998%)], were used for gas sorption experiments. Adsorption experiments (up to 1 bar) for different pure gases were performed using a Micromeritics 3Flex 3500 surface area and pore size analyzer. Before sorption measurements, activation of SIFSIX-18-Ni was achieved by degassing the methanol-exchanged sample on a SmartVacPrep using dynamic vacuum and heating for 4 hours (sample was heated from room temperature to 348 K with a ramp rate of 5°C). Brunauer-Emmett-Teller (BET) surface areas were determined from the N_2 adsorption isotherms at 77 K using the Micromeritics Microactive software except for NbOFFIVE-1-Ni and TIFSIX-3-Ni, whose BET surface areas were calculated from their 298 K CO_2 adsorption isotherms. About 200 mg of activated samples was used for the measurements. Very low pressure CO_2 measurements were performed using a Micromeritics 3Flex surface area and pore size analyzer at 273, 283, and 298 K. A Julabo temperature controller was used to maintain a constant temperature in the bath throughout the experiment. Bath temperatures of 273, 283, and 298 K were precisely controlled with a Julabo ME (v.2) recirculating control system containing a mixture of ethylene glycol and water. The low temperatures at 77 and 195 K were controlled using a 4-liter Dewar flask filled with liquid N_2 and dry ice/acetone, respectively. O_2 adsorption isotherm at 77 K was measured up to ~146 mmHg, because the saturation vapor pressure (P_0) of O_2 at 77 K is 147.8 mmHg.

Breakthrough experiments

In typical breakthrough experiments, ~0.3, 0.33, and 0.24 g of pre-activated SIFSIX-18-Ni-β, NbOFFIVE-1-Ni, and ZIF-8, respectively, and ~0.31 g of Zeolite 13X and TIFSIX-3-Ni were placed in quartz tubing (8 mm diameter) to form a fixed bed. First, the adsorbent bed was purged under a 25 cm^3 min^{-1} flow of He gas at 333 K for 30 min before breakthrough experiment. Upon cooling to room temperature, the gas flow was switched to the desired gas mixture at a particular flow rate (the respective flow rates are mentioned in the figure captions and in table S4). Here, trace CO_2/N_2 (~1000, 3000, 5000, and 10,000 ppm)/(99.9, 99.7, 99.5, and 99%, respectively) breakthrough experiments were conducted at 298 K. The outlet composition was continuously monitored using a Hiden HPR-20 quartz inert capillary mass spectrometer until complete breakthrough was achieved. After each dry and wet breakthrough experiment, the packed column bed was regenerated at 403 K (SIFSIX-18-Ni-β, NbOFFIVE-1-Ni, ZIF-8, and TIFSIX-3-Ni) and 573 K (Zeolite 13X) with constant He flow (25 cm^3 min^{-1}) for 120 min to ensure complete sample regeneration. Experiments in the presence of 74% RH were performed by passing the gas stream through a water vapor saturator at 298 K.

SUPPLEMENTARY MATERIALS

Supplementary material for this article is available at http://advances.sciencemag.org/cgi/content/full/5/11/eaax9171/DC1

Supplementary Materials and Methods

Supplementary Text

Fig. S1. PXRD of SIFSIX-18-Ni.

Fig. S2. Variable temperature PXRD of SIFSIX-18-Ni.

Fig. S3. Comparison of experimental PXRD profiles for SIFSIX-18-Ni-α, SIFSIX-18-Ni-β, and SIFSIX-18-Ni-γ with their calculated patterns and related polymorphs (24) (all recorded at 298 K).

Fig. S4. Comparison of experimental PXRD profiles for SIFSIX-18-Ni-β, SIFSIX-18-Ni-β (activated, before dosing CO_2), and SIFSIX-18-Ni-β (dosed with 1 bar CO_2 at 303 K) with the calculated pattern of SIFSIX-18-Ni-β.

Fig. S5. Comparison of experimental PXRD profiles for SIFSIX-18-Ni-α, SIFSIX-18-Ni-β, and SIFSIX-18-Ni-β (activated, before dosing H_2O).

Fig. S6. Particle size distribution around the mean diameter (~13.94 μm) range of SIFSIX-18-Ni-β.

Fig. S7. Thermogravimetric analysis profiles of SIFSIX-18-Ni.

Fig. S8. CO_2 sorption isotherms for SIFSIX-18-Ni-β; inset: low pressure range until 0.01 bar.

Fig. S9. Low-temperature CO_2, N_2, and O_2 sorption isotherms for SIFSIX-18-Ni-β.

Fig. S10. CO_2 and N_2 sorption isotherms for SIFSIX-18-Ni-β.

Fig. S11. CO_2 and O_2 sorption isotherms for SIFSIX-18-Ni-β.

Fig. S12. CO_2 sorption isotherms at 298 K for SIFSIX-18-Ni-α (only subjected to evacuation after MeOH washing of precursor, i.e., no heating), SIFSIX-18-Ni-β, and SIFSIX-18-Ni-γ.

Fig. S13. CO_2 and N_2 sorption isotherms for Mg-MOF-74.

Fig. S14. CO_2 and N_2 sorption isotherms for Zeolite 13X.

Fig. S15. CO_2 and N_2 sorption isotherms for SIFSIX-3-Ni.

Fig. S16. CO_2 and N_2 sorption isotherms for NbOFFIVE-1-Ni.

Fig. S17. CO_2 and N_2 sorption isotherms for TIFSIX-3-Ni.

Fig. S18. CO_2 and N_2 sorption isotherms for ZIF-8.

Fig. S19. Fitting of the isotherm data for SIFSIX-18-Ni-β to the virial equation.

Fig. S20. Fitting of the isotherm data for ZIF-8 to the virial equation.

Fig. S21. H_2O sorption isotherms for SIFSIX-18-Ni-β compared with other HUMs (all recorded at 298 K).

Fig. S22. Sorption isotherms (298 K) for CO_2 and H_2O for SIFSIX-18-Ni-β compared with other HUMs; pressure range until 0.03 bar i.e. saturation pressure of H_2O at 298 K.

Fig. S23. H_2O sorption isotherms (298 K) of SIFSIX-18-Ni-β for vacuum DVS and intrinsic DVS experiments.

Fig. S24. H_2O sorption isotherms of SIFSIX-18-Ni-β recorded at different temperatures by intrinsic DVS experiments.

Fig. S25. Humidity-dependent CO_2/H_2O selectivities (S_{CW}) for SIFSIX-18-Ni-β at 298 K.

Fig. S26. CO_2/H_2O selectivities (S_{CW}) for SIFSIX-18-Ni-β under different CO_2 concentrations at 298 K.

Fig. S27. 0.1/99.9 (v/v) CO_2/N_2 breakthrough profiles and CO_2 effluent purities for SIFSIX-18-Ni-β under dry and 74% RH conditions; flow rate = 20 cm^3 min^{-1}.

Fig. S28. 0.3/99.7 (v/v) CO_2/N_2 breakthrough profiles and CO_2 effluent purities for SIFSIX-18-Ni-β under dry and 74% RH conditions; flow rate = 20 cm^3 min^{-1}.

Fig. S29. 0.1/99.9 (v/v) CO_2/N_2 breakthrough profiles and CO_2 effluent purities for NbOFFIVE-1-Ni under dry and 74% RH conditions; flow rate = 20 cm^3 min^{-1}.

Fig. S30. 0.3/99.7 (v/v) CO_2/N_2 breakthrough profiles and CO_2 effluent purities for NbOFFIVE-1-Ni under dry and 74% RH conditions; flow rate = 20 cm^3 min^{-1}.

Fig. S31. 0.1/99.9 (v/v) CO_2/N_2 breakthrough profiles and CO_2 effluent purities for Zeolite 13X under dry and 74% RH conditions; flow rate = 20 cm^3 min^{-1}.

Fig. S32. 0.3/99.7 (v/v) CO_2/N_2 breakthrough profiles and CO_2 effluent purities for Zeolite 13X under dry and 74% RH conditions; flow rate = 20 cm^3 min^{-1}.

Fig. S33. 0.1/99.9 (v/v) CO_2/N_2 breakthrough profiles and CO_2 effluent purities for SIFSIX-3-Ni under dry and 74% RH conditions; flow rate = 20 cm^3 min^{-1}.

Fig. S34. 0.3/99.7 (v/v) CO_2/N_2 breakthrough profiles and CO_2 effluent purities for SIFSIX-3-Ni under dry and 74% RH conditions; flow rate = 20 cm^3 min^{-1}.

Fig. S35. 0.1/99.9 (v/v) CO_2/N_2 breakthrough profiles and CO_2 effluent purities for TIFSIX-3-Ni under dry and 74% RH conditions; flow rate = 20 cm^3 min^{-1}.

Fig. S36. 0.3/99.7 (v/v) CO_2/N_2 breakthrough profiles and CO_2 effluent purities for TIFSIX-3-Ni under dry and 74% RH conditions; flow rate = 20 cm^3 min^{-1}.

Fig. S37. 1000 ppm CO_2/N_2 (v/v = 0.1/99.9%) breakthrough profiles for ZIF-8 under dry condition, flow rate = 20 cm^3 min^{-1}.

Fig. S38. 3000 ppm CO_2/N_2 (v/v = 0.3/99.7%) breakthrough profiles for ZIF-8 under dry condition, flow rate = 20 cm^3 min^{-1}.

Fig. S39. 0.5/99.5 (v/v) CO_2/N_2 breakthrough profiles and CO_2 effluent purities for SIFSIX-18-Ni-β and NbOFFIVE-1-Ni under dry and 74% RH conditions; flow rate = 10 cm^3 min^{-1}.

Fig. S40. 1/99 (v/v) CO_2/N_2 breakthrough profiles and CO_2 effluent purities for SIFSIX-18-Ni-β and NbOFFIVE-1-Ni under dry and 74% RH conditions; flow rate = 10 cm^3 min^{-1}.

Fig. S41. Temperature-programmed desorption plot of DAC of CO_2 experiment for SIFSIX-18-Ni-β.

Fig. S42. PXRD profiles for SIFSIX-18-Ni before and after accelerated stability test.

Fig. S43. BET surface areas as obtained from 77 K N_2 adsorption isotherms for SIFSIX-18-Ni and other adsorbents, after accelerated stability test.

Fig. S44. CO_2 adsorption isotherms (298 K) for SIFSIX-18-Ni after accelerated stability test.

Fig. S45. IAST selectivity comparison for benchmark physisorbents at CO_2 (500 ppm): N_2 binary mixture; results for SIFSIX-18-Ni-β not included as partial sieving effect is observed.

Fig. S46. IAST selectivities found in SIFSIX-18-Ni-β for CO_2/O_2 binary mixtures with varying CO_2 concentrations.

Fig. S47. FTIR spectra of SIFSIX-18-Ni: as-synthesized, activated (β), after CO_2 sorption, after H_2O sorption, and after 1-hour CO_2 dosing at 1 bar.

Fig. S48. 0.1/99.9 (v/v) CO_2/N_2 adsorption-desorption recyclability over 6 consecutive cycles for SIFSIX-18-Ni-β under dry and 74% RH conditions.

Fig. S49. 0.3/99.7 (v/v) CO_2/N_2 adsorption-desorption recyclability over 6 consecutive cycles for SIFSIX-18-Ni-β under dry and 74% RH conditions.

Fig. S50. 0.5/99.5 (v/v) CO_2/N_2 adsorption-desorption recyclability over 6 consecutive cycles for SIFSIX-18-Ni-β under dry and 74% RH conditions.

Fig. S51. 1/99 (v/v) CO_2/N_2 adsorption-desorption recyclability over 6 consecutive cycles for SIFSIX-18-Ni-β under dry and 74% RH conditions.

Fig. S52. CO_2 adsorption-desorption recyclability over 100 cycles for SIFSIX-18-Ni-β (1.0 bar CO_2; desorption at 348 K): for each cycle, 60 min of isothermal (303 K) gravimetric CO_2 uptake recorded on the activated sample.

Fig. S53. Comparison of gravimetric C-capture kinetics in SIFSIX-18-Ni-β and TEPA-SBA-15 under dry conditions.

Fig. S54. Comparison of gravimetric C-capture kinetics in SIFSIX-18-Ni-β and TEPA-SBA-15 under wet conditions.

Fig. S55. Diffractograms for the Le Bail refinement of SIFSIX-18-Ni-α.

Fig. S56. Diffractograms for the Rietveld refinement of SIFSIX-18-Ni-β.

Fig. S57. Equilibrated structure of CO_2 molecules residing in the cavity of SIFSIX-18-Ni-β corresponding to a loading of 2 CO_2 per formula unit.

Fig. S58. Scheme of the coupled gas mixing system, TGA-based gas uptake analysis, and breakthrough separation analysis unit.

Table S1. Calculated S_{CW} at 74% RH.

Table S2. Fitting parameters for SIFSIX-18-Ni-β.

Table S3. Fitting parameters for ZIF-8.

Table S4. Dynamic breakthrough experiment details of CO_2/N_2 at 298 K and 1 bar.

Table S5. Crystallographic data for SIFSIX-18-Ni.

References (41–45)

REFERENCES AND NOTES

1. The NOAA *Annual Greenhouse Gas Index* (AGGI) (U.S. Department of Commerce, 2017); https://www.esrl.noaa.gov/gmd/aggi/aggi.html.

2. International Energy Agency, *Global Energy & CO₂ Status Report* (International Energy Agency, 2017).

3. N. MacDowell, P. S. Fennell, N. Shah, G. C. Maitland, The role of CO_2 capture and utilization in mitigating climate change. *Nat. Clim. Change* **7**, 243 (2017).

4. National Research Council, *The Airliner Cabin Environment and the Health of Passengers and Crew* (The National Academies Press, 2002), p. 344.

5. A. Stankovic, D. Alexander, C. M. Oman, J. Schneiderman, *A Review of Cognitive and Behavioral Effects of Increased Carbon Dioxide Exposure in Humans 2016–2017* (NASA/TM-2016-219277, NASA, 2016).

6. T. A. Jacobson, J. S. Kler, M. T. Hernke, R. K. Braun, K. C. Meyer, W. E. Funk, Direct human health risks of increased atmospheric carbon dioxide. *Nat. Sustain.* **2**, 691–701 (2019).

7. M. E. Boot-Handford, J. C. Abanades, E. J. Anthony, M. J. Blunt, S. Brandani, N. Mac Dowell, J. R. Fernández, M. C. Ferrari, R. Gross, J. P. Hallett, R. S. Haszeldine, P. Heptonstall, A. Lyngfelt, Z. Makuch, E. Mangano, R. T. J. Porter, M. Pourkashanian, G. T. Rochelle, N. Shah, J. G. Yao, P. S. Fennell, Carbon capture and storage update. *Energy Environ. Sci.* **7**, 130–189 (2014).

8. P. Smith, S. J. Davis, F. Creutzig, S. Fuss, J. Minx, B. Gabrielle, E. Kato, R. B. Jackson, A. Cowie, E. Kriegler, D. P. van Vuuren, J. Rogelj, P. Ciais, J. Milne, J. G. Canadell, D. McCollum, G. Peters, R. Andrew, V. Krey, G. Shrestha, P. Friedlingstein, T. Gasser, A. Grübler, W. K. Heidug, M. Jonas, C. D. Jones, F. Kraxner, E. Littleton, J. Lowe, J. Roberto Moreira, N. Nakicenovic, M. Obersteiner, A. Patwardhan, M. Rogner, E. Rubin, A. Sharifi, A. Torvanger, Y. Yamagata, J. Edmonds, C. Yongsung, Biophysical and economic limits to negative CO_2 emissions. *Nat. Clim. Change* **6**, 42–50 (2015).

9. D. M. D'Alessandro, B. Smit, J. R. Long, Carbon dioxide capture: Prospects for new materials. *Angew. Chem. Int. Ed.* **49**, 6058–6082 (2010).

10. S.-C. Hu, A. Shiue, S.-M. Chang, Y.-T. Chang, C.-H. Tseng, C.-C. Mao, A. Hsieh, A. Chan, Removal of carbon dioxide in the indoor environment with sorption-type air filters. *Int. J. Low-Carbon Technol.* **12**, 330–334 (2017).

11. J. Blamey, E. J. Anthony, J. Wang, P. S. Fennell, The calcium looping cycle for large-scale CO_2 capture. *Prog. Energy Combust. Sci.* **36**, 260–279 (2010).

12. E. S. Sanz-Pérez, C. R. Murdock, S. A. Didas, C. W. Jones, Direct capture of CO2 from ambient air. *Chem. Rev.* **116**, 11840–11876 (2016).

13. M. Oschatz, M. Antonietti, A search for selectivity to enable CO2 capture with porous adsorbents. *Energ. Environ. Sci.* **11**, 57–70 (2018).

14. A. Heydari-Gorji, A. Sayari, Thermal, oxidative, and CO_2-induced degradation of supported Polyethylenimine Adsorbents. *Ind. Eng. Chem. Res.* **51**, 6887–6894 (2012).

15. J. J. Perry Iv, J. A. Perman, M. J. Zaworotko, Design and synthesis of metal–organic frameworks using metal–organic polyhedra as supermolecular building blocks. *Chem. Soc. Rev.* **38**, 1400–1417 (2009).

16. R. Kitaura, K. Seki, G. Akiyama, S. Kitagawa, Porous coordination-polymer crystals with gated channels specific for supercritical gases. *Angew. Chem. Int. Ed.* **42**, 428–431 (2003).

17. M. Schroeder, *Functional Metal–Organic Frameworks: Gas Storage, Separation and Catalysis* (Springer-Verlag, 2010).

18. D. G. Madden, H. S. Scott, A. Kumar, K.-J. Chen, R. Sanii, A. Bajpai, M. Lusi, T. Curtin, J. J. Perry, M. J. Zaworotko, Flue-gas and direct-air capture of CO_2 by porous metal-organic materials. *Philos. Trans. A Math. Phys. Eng. Sci.* **375**, 20160025 (2017).

19. A. Kumar, Direct air capture of CO_2 by physisorbent materials. *Angew. Chem. Int. Ed.* **54**, 14372–14377 (2015).

20. H. S. Scott, A. Bajpai, K.-J. Chen, T. Pham, B. Space, J. J. Perry, M. J. Zaworotko, Novel mode of 2-fold interpenetration observed in a primitive cubic network of formula $[Ni(1,2-bis(4-pyridyl)acetylene)_2(Cr_2O_7)]_n$. *Chem. Commun.* **51**, 14832–14835 (2015).

21. P. Nugent, Y. Belmabkhout, S. D. Burd, A. J. Cairns, R. Luebke, K. Forrest, T. Pham, S. Ma, B. Space, L. Wojtas, M. Eddaoudi, M. J. Zaworotko, Porous materials with optimal adsorption thermodynamics and kinetics for CO_2 separation. *Nature* **495**, 80–84 (2013).

22. X. Cui, K. Chen, H. Xing, Q. Yang, R. Krishna, Z. Bao, H. Wu, W. Zhou, X. Dong, Y. Han, B. Li, Q. Ren, M. J. Zaworotko, B. Chen, Pore chemistry and size control in hybrid porous materials for acetylene capture from ethylene. *Science* **353**, 141–144 (2016).

23. J. G. Nguyen, S. M. Cohen, Moisture-Resistant and Superhydrophobic Metal–Organic Frameworks Obtained via Postsynthetic Modification. *J. Am. Chem. Soc.* **132**, 4560–4561 (2010).

24. V. V. Ponomarova, V. V. Komarchuk, I. Boldog, H. Krautscheid, K. V. Domasevitch, Modular construction of 3D coordination frameworks incorporating SiF_6^{2-} links: Accessing the significance of $[M(pyrazole)_4(SiF_6)]$ synthon. *CrstEngComm* **15**, 8280–8287 (2013).

25. D. Britt, D. Tranchemontagne, O. M. Yaghi, Metal-organic frameworks with high capacity and selectivity for harmful gases. *Proc. Natl. Acad. Sci. U.S.A.* **105**, 11623–11627 (2008).

26. K. S. Park, Z. Ni, A. P. Cote, J. Y. Choi, R. Huang, F. J. Uribe-Romo, H. K. Chae, M. O'Keeffe, O. M. Yaghi, Exceptional chemical and thermal stability of zeolitic imidazolate frameworks. *Proc. Natl. Acad. Sci. U.S.A.* **103**, 10186–10191 (2006).

27. S. Cavenati, C. A. Grande, A. E. Rodrigues, Adsorption equilibrium of methane, CARBON dioxide, and nitrogen on zeolite 13X at high Pressures. *J. Chem. Eng. Data* **49**, 1095–1101 (2004).

28. P. M. Bhatt, Y. Belmabkhout, A. Cadiau, K. Adil, O. Shekhah, A. Shkurenko, L. J. Barbour, M. Eddaoudi, A Fine-Tuned Fluorinated MOF Addresses the Needs for Trace CO2 Removal and Air Capture Using Physisorption. *J. Am. Chem. Soc.* **138**, 9301–9307 (2016).

29. A. Kumar, C. Hua, D. G. Madden, D. O'Nolan, K. J. Chen, L. A. J. Keane, J. J. Perry, M. J. Zaworotko, Hybrid ultramicroporous materials (HUMs) with enhanced stability and trace carbon capture performance. *Chem. Commun.* **53**, 5946–5949 (2017).

30. N. C. Burtch, H. Jasuja, K. S. Walton, Water stability and adsorption in metal-organic frameworks. *Chem. Rev.* **114**, 10575–10612 (2014).

31. A. Zhao, A. Samanta, P. Sarkar, R. Gupta, carbon dioxide adsorption on amine-impregnated mesoporous SBA-15 Sorbents: Experimental and kinetics study. *Ind. Eng. Chem. Res.* **52**, 6480–6491 (2013).

32. A. L. Myers, J. M. Prausnitz, Thermodynamics of mixed-gas adsorption. *AIChE J.* **11**, 121–127 (1965).

33. K. C. Waterman, Understanding and predicting pharmaceutical product shelf-life, in *Handbook of Stability Testing in Pharmaceutical Development* (Springer, 2009), pp. 115–135.

34. S. Kitagawa, Porous materials and the age of gas. *Angew. Chem. Int. Ed.* **54**, 10686–10687 (2015).

35. D. O'Nolan, A. Kumar, M. J. Zaworotko, Water vapor sorption in hybrid pillared square grid materials. *J. Am. Chem. Soc.* **139**, 8508–8513 (2017).

36. H. Jasuja, N. C. Burtch, Y. Huang, Y. Cai, K. S. Walton, Kinetic water stability of an isostructural family of zinc-based pillared metal–organic frameworks. *Langmuir* **29**, 633–642 (2013).

37. J. Liu, Y. Wei, Y. Zhao, Trace carbon dioxide capture by metal–organic frameworks. *ACS Sustain. Chem. Eng.* **7**, 82–93 (2018).

38. R. Vaidhyanathan, S. S. Iremonger, G. K. H. Shimizu, P. G. Boyd, S. Alavi, T. K. Woo, Direct observation and quantification of CO2 Binding within an amine-functionalized nanoporous solid. *Science* **330**, 650–653 (2010).

39. S. M. Whitney, R. L. Houtz, H. Alonso, Advancing our understanding and capacity to engineer nature's CO_2-sequestering enzyme, Rubisco. *Plant Physiol.* **155**, 27–35 (2011).

40. M. van Lun, J. S. Hub, D. van der Spoel, I. Andersson, CO_2 and O_2 distribution in Rubisco suggests the small subunit functions as a CO_2 reservoir. *J. Am. Chem. Soc.* **136**, 3165–3171 (2014).

41. International Council for Harmonisation of Technical Requirements for Pharmaceuticals for Human Use (ICH) Guideline, *ICH Q1A (R2): Stability Testing of New Drug Substances and Drug Products* (European Medicines Agency, 2003).

42. P. E. Kruger, B. Moubaraki, G. D. Fallon, K. S. Murray, Tetranuclear copper(II) complexes incorporating short and long metal–metal separations: Synthesis, structure and magnetism. *J. Chem. Soc. Dalton Trans.* **2000**, 713–718 (2000).

43. J. Hutter, M. Iannuzzi, F. Schiffmann, J. VandeVondele, cp2k: Atomistic simulations of condensed matter systems. *Wiley Interdiscip. Rev. Comput. Mol. Sci.* **4**, 15–25 (2014).

44. A. K. Rappe, C. J. Casewit, K. S. Colwell, W. A. Goddard, W. M. Skiff, UFF, a full periodic table force field for molecular mechanics and molecular dynamics simulations. *J. Am. Chem. Soc.* **114**, 10024–10035 (1992).

45. A. L. Mullen, T. Pham, K. A. Forrest, C. R. Cioce, K. McLaughlin, B. Space, A polarizable and transferable PHAST CO_2 potential for materials simulation. *J. Chem. Theory Comput.* **9**, 5421–5429 (2013).